

# One-pot Synthesis of Mixed-phase Pd-Ru/C as Efficient Catalysts for Electro-oxidation of Formic Acid

Mingsheng Wei<sup>1,2,\*</sup>, Chiajen Hsu<sup>2</sup> and Fuqiang Liu<sup>2,\*</sup>

<sup>1</sup>School of Physics and Electronic Engineering, Jiangsu Normal University, Xuzhou 221116, China

<sup>2</sup>Electrochemical Energy Laboratory, Department of Materials Science and Engineering, University of Texas at Arlington, Arlington, TX 76019, USA

\*E-mail: [weims@jsnu.edu.cn](mailto:weims@jsnu.edu.cn); [fuqiang@uta.edu](mailto:fuqiang@uta.edu)

Received: 10 December 2015 / Accepted: 30 December 2015 / Published: 1 February 2016

---

A series of bimetallic Pd<sub>x</sub>Ru<sub>y</sub>/C (x:y = 4:1, 2:1, 1:1, and 1:2) nanoparticles have been synthesized by reducing PdCl<sub>2</sub> and RuCl<sub>3</sub> on carbon support by sodium borohydride for electrochemical oxidation of formic acid. Particularly, the extent of PdRu alloying was intentionally kept low and constant (around 2%) in order to understand the effect of Ru composition in mixed-phase PdRu catalysts. The catalysts were characterized by X-ray diffraction (XRD), transmission electron microscopy (TEM), and electrochemical measurements. XRD analysis confirmed the mixed-phase structure of the Pd-Ru nanoparticles. TEM images displayed well-distributed Pd-Ru nanoparticles on the carbon support with an average particle size around 4.3 nm. The Pd<sub>x</sub>Ru<sub>y</sub>/C nanoparticles, especially the Pd<sub>2</sub>Ru/C, were found to exhibit superior formic acid oxidation activity with lower CO-stripping onset potentials and long-cycle durability compared to the commercial Pd/C. The interaction between boundary sites at their individual phases in the mixed-phase PdRu catalysts resulted in the observed significant electrochemical improvement. These results suggested potential application of these Pd-Ru/C materials as catalysts in direct formic acid fuel cells.

---

**Keywords:** PdRu, Nanoparticle, Formic acid oxidation, CO-stripping, Fuel cell

## 1. INTRODUCTION

Direct formic acid fuel cells (DFAFCs) compared to direct methanol fuel cells (DMFCs) display promising advantages [1] such as low fuel crossover through membrane, suppressed fuel pollution, and mitigated catalyst poison [2], therefore have been considered as one of the promising alternative energy sources. Many efforts developing DFAFCs have been devoted to enhancing formic acid oxidation (FAO) efficiency and anti-poison ability of catalysts. Liu et al. [3] studied electrochemical FAO using Pt/C and Pd/C, and found that superior performance of Pd/C was attributed

to efficient carbon monoxide (CO) removal from the catalyst surface. Besides, Pd and bimetallic Pd-based catalysts [4] have been widely studied for FAO because of a direct dehydrogenation pathway, i.e., direct conversion of formic acid to CO<sub>2</sub> [5] on Pd.

Recent works on Pd-based bimetallic catalysts have focused on different transition metals with varying d-band vacancy that may alter the electronic state of Pd. Wang et al. [6] studied FAO on PdCo/C, and reported 1.12 and 3.25 times higher peak and stabilized oxidation current densities, respectively, than those of commercial Pd/C. Du et al. [7] observed a direct FAO pathway on PdNi<sub>2</sub> alloyed catalysts which also showed higher FAO activity. In addition, Xu et al. [8] suggested that FAO on nanoporous PdCu alloys with less than 50 at.% of Cu proceeds via a direct pathway; while FAO is through a pathway that generates CO when Cu content is more than 70 at.%. The fundamental change in reaction pathways originates from varied bonding strength of reaction intermediates (e.g., formate, hydroxyl [9], and CO), which may result in an increase of FAO efficiency [10].

Regarding the anti-poison mechanism of the bimetallic alloys, CO as an intermediate in FAO reactions adsorbs on the surface of Pd and is oxidized with the help of other metals at lower potentials to free more surface sites for the subsequent FAO reaction. In general, these metals, such as Ir [11] and Ru [12-19], could supply oxygen-containing species to Pd via a spillover route and help oxidize the adsorbed CO in a so-called bi-functional mechanism. For example, Wu et al. [18] discussed the impact of mixed-phase PdRu bimetallic structures for FAO and found that Pd-Ru nanoparticles showed higher electrochemical FAO activity than monometallic Ru or Pd nanoparticles. Liu et al. [14] compared different molar ratios of Pd to Ru (5:1, 3:1, 1:1) in bimetallic PdRu catalysts for FAO, and found that Pd<sub>5</sub>Ru/C exhibited the best catalytic activities. Though bimetallic PdRu catalyst seems a promising candidate to enhance FAO activity, the origin of its enhanced activity still seems controversial. It has been suggested that non-alloyed bimetallic mixture may be more electrochemically active due to boundary sites between individual phases [18, 20]. However, a systemic study on impacts of Ru to Pd-Ru/C for electrochemical FAO is rare, especially for higher Ru molar ratios. In the study conducted by Liu et al. [14], both Ru content and the extent of PdRu alloying were varied (from 4% to 21%); therefore, the observed electrocatalytic performance of their PdRu catalysts could not be solely accounted for. The work performed by Wu et al. [18] only focused on Pd<sub>0.5</sub>Ru<sub>0.5</sub> and the extent of alloying was unknown.

In this work, we conducted a systemic investigation on impacts of Ru to bimetallic Pd-Ru/C nanoparticles in FAO reaction. Most important, the extent of PdRu alloying was intentionally kept low and constant (around 2%) in order to understand purely the effect of Ru composition in mixed-phase PdRu catalysts. Herein, we reported a facile method to synthesize the bimetallic Pd-Ru/C nanoparticles with controllable Pd to Ru molar ratios. The physical properties and electrochemical FAO activity of the Pd-Ru alloy were investigated. Efforts were also taken to understand the remarkable enhancement in catalytic activities and long-term durability of the Pd-Ru/C compared to the commercial Pd/C.

## 2. EXPERIMENTAL SECTION

The method reported by Wang et al. [21] was modified to synthesize the Pd<sub>x</sub>Ru<sub>y</sub>/C (x and y are denoted as molar ratios of the two metals: x:y = 4:1, 2:1, 1:1, and 1:2), and Ru/C catalysts. In brief,

solutions of PdCl<sub>2</sub> (Aldrich) and RuCl<sub>3</sub> (Aldrich) in 0.4 M citric acid (Aldrich) were first prepared separately. Here the citric acid was used as the stabilizing agent [5] to prevent reduction of Pd. According to the designed molar ratios, different amounts of the PdCl<sub>2</sub> and RuCl<sub>3</sub> solutions were mixed with Ketjen carbon black (EC300 J, Akzo Nobel Chemicals) and stirred for 2 hrs. Subsequently, 0.1 M NaBH<sub>4</sub> (Sigma) as the reducing agent was added dropwise into the mixed solutions under vigorous stirring. Finally, the resulted catalyst was filtered and thoroughly washed with DI water, before being dried in an oven at 80 °C overnight. Note that no high-temperature annealing was performed so that alloying between Pd and Ru could be controlled

Crystalline structures of the synthesized catalysts were characterized using a X-ray diffractometer (Siemens D500) equipped with a Cu K $\alpha$  source at a scan rate of 1.0 °·min<sup>-1</sup> from 10° to 80°. Particle size and nanostructures were investigated using a high resolution transmission electron microscope (HR-TEM, Hitachi H-9500) at 300 kV accelerated voltage. Electrochemical measurements were conducted at ambient temperature by a PARSTAT 2273 potentiostat (Princeton Applied Research) in a conventional three-electrode configuration consisting a glassy carbon working electrode (geometric area: 0.19635 cm<sup>2</sup>, Pine Instrument Company), a Pt mesh counter electrode, and a normal hydrogen electrode (NHE) as the reference electrode. Briefly, the electrodes on the glassy carbon were first prepared by taking 15  $\mu$ l ink from a mixed solution of 10 mg catalysts in 20 ml DI water and were then dried under an infrared lamp. After that, 4.7 ml Nafion solution (Ion Power Inc.) was coated onto the top of the catalysts.

Cyclic voltammetry (CV) scanning from 0.03 V to 1.2 V at a rate of 20 mV s<sup>-1</sup> was employed to study electrochemical characteristics of the prepared samples. Hydrogen adsorption area during the cathodic scan was used to calculate the electrochemical surface area (ECSA) according to the following equation:

$$ECSA = \frac{Q_H}{Q_C [Pd]} \quad (1)$$

where Q<sub>H</sub> (mC cm<sup>-2</sup>) is the charge under the hydrogen adsorption peak, [Pd] is the Pd loading on the working electrode, and Q<sub>C</sub> is 0.21 mC cm<sup>-2</sup> corresponding to a monolayer of hydrogen on Pd. The calculated ECSA values are 51.94 m<sup>2</sup> g<sup>-1</sup> (Pd<sub>4</sub>Ru/C), 55.54 m<sup>2</sup> g<sup>-1</sup> (Pd<sub>2</sub>Ru/C), 62.58 m<sup>2</sup> g<sup>-1</sup> (PdRu/C), 55.20 m<sup>2</sup> g<sup>-1</sup> (PdRu<sub>2</sub>/C), and 50.22 m<sup>2</sup> g<sup>-1</sup> (commercial Pd/C, Sigma).

The electronic characteristics of the catalyst surface was probed by CO-stripping CV. CO was first absorbed on the catalyst surface at 0.2 V for 15 min in CO-saturated 0.1 M HClO<sub>4</sub> solution and then was electrochemically removed by scanning from 0.03 V to 1.2 V at 20 mV s<sup>-1</sup> in Ar-saturated 0.1 M HClO<sub>4</sub> solution. Electrochemical stability tests were performed up to 100 CV cycles in a mixed solution of 0.1 M formic acid and 0.1 M HClO<sub>4</sub> at a scan rate of 50 mV s<sup>-1</sup>, and the electrochemical currents were compared to the beginning-of-life performance.

### 3. RESULTS AND DISCUSSION

The XRD patterns of the Pd<sub>x</sub>Ru<sub>y</sub>/C, Ru/C, and commercial Pd/C are shown in Fig. 1. A broad peak at around 25° for all the catalysts is assigned to the carbon support. The Pd peaks at 40.64°,

46.15°, 68.27° correspond to (111), (200) and (220) planes in the fcc structure, respectively. In addition, the strong Ru reflection peak at 43.67° corresponds to the (101) plane.

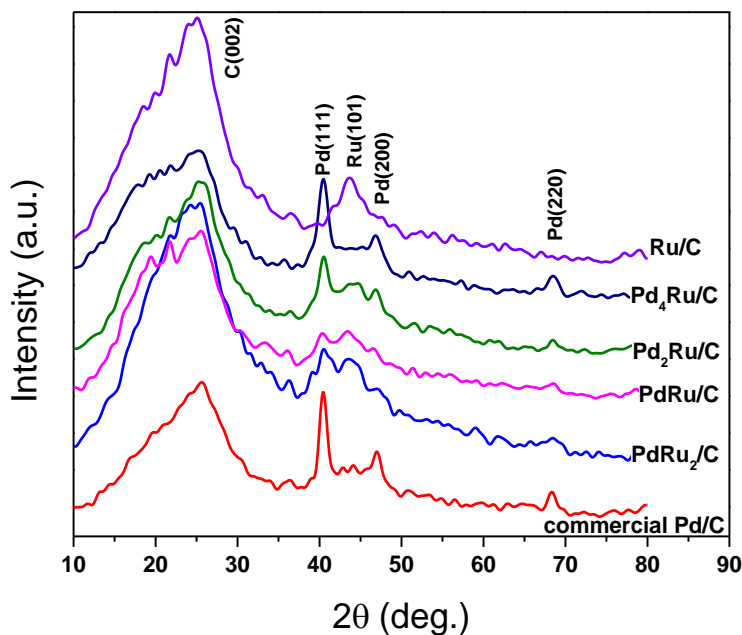


**Figure 1.** XRD patterns of Pd/C, Pd<sub>x</sub>Ru<sub>y</sub>/C, and Ru/C catalysts

With increasing Ru molar ratio in the bimetallic Pd<sub>x</sub>Ru<sub>y</sub> catalysts, the intensity of Pd (111) and (200) signals drops; the two peaks seem to merge into a broader one due to overlap with Ru (101). In order to identify the formation of Pd<sub>x</sub>Ru<sub>y</sub> alloy, the Pd (220) was used to calculate the lattice constant and compared with that of the Pd/C catalyst. Careful observation of the Pd (220) angles for the samples indicates a slight shift to higher angles: commercial Pd/C at 68.1°, Pd<sub>4</sub>Ru/C at 68.42°, Pd<sub>2</sub>Ru/C at 68.48°, PdRu/C at 68.66°, and PdRu<sub>2</sub>/C at 68.73°, due to the lattice contraction caused by the substitution of Ru atoms into the Pd fcc lattice [14]. According to the Bragg’s Law, the lattice constant of Pd (220) was calculated by the following equation:

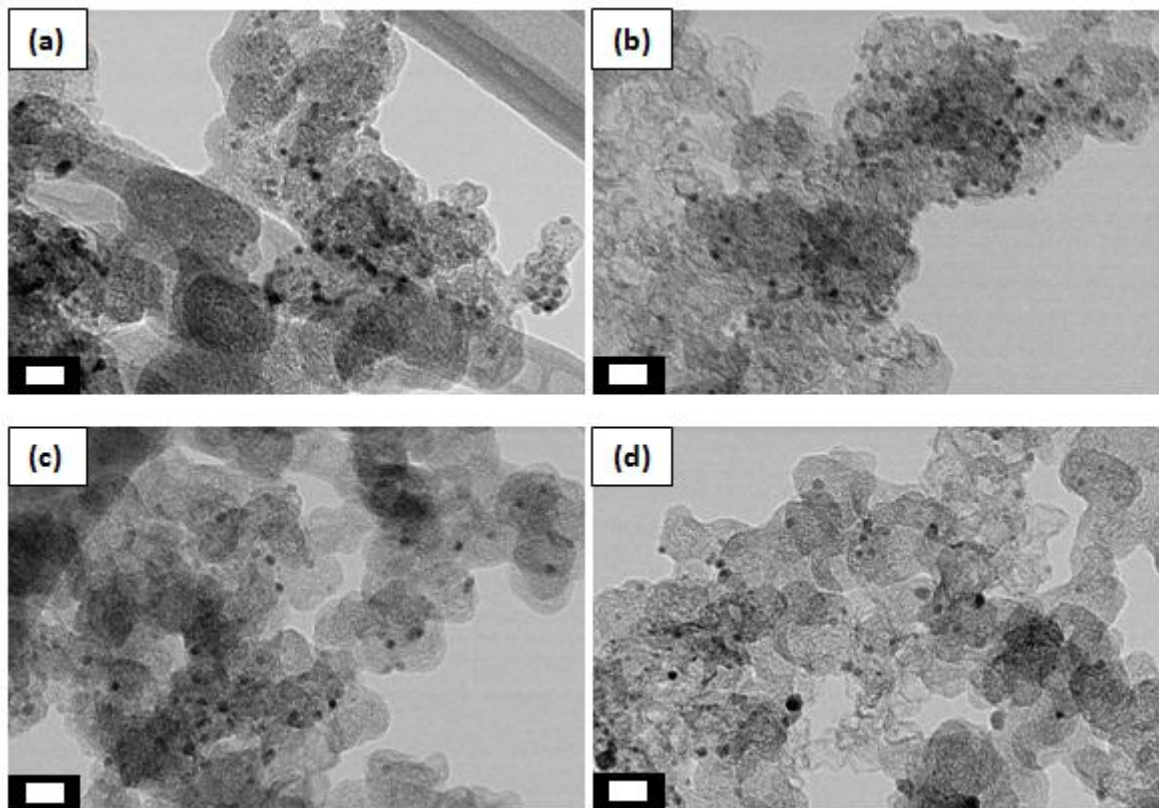
$$a = \frac{\sqrt{h^2 + k^2 + l^2} \times \lambda}{2 \sin \theta} \tag{2}$$

where *a* is the lattice parameter,  $\lambda$  is the incident wavelength (0.154 nm),  $\theta$  is the diffraction angle, and h, k, and l are the Miller indices of the (220) plane. Herein, the lattice parameters of commercial Pd/C, Pd<sub>4</sub>Ru/C, Pd<sub>2</sub>Ru/C, PdRu/C, and PdRu<sub>2</sub>/C were calculated to be 0.3890 nm, 0.3874 nm, 0.3871 nm, 0.3862 nm and 0.3858 nm, respectively, clearly confirming that the Pd lattice shrinkage by Ru is not significant. Based on the lattice constants, the extent of alloying (*x*<sub>PdRu</sub>) was calculated using Vegard’s law:

$$a_{PdRu} = a_{Pd} - k \cdot x_{PdRu} \tag{3}$$

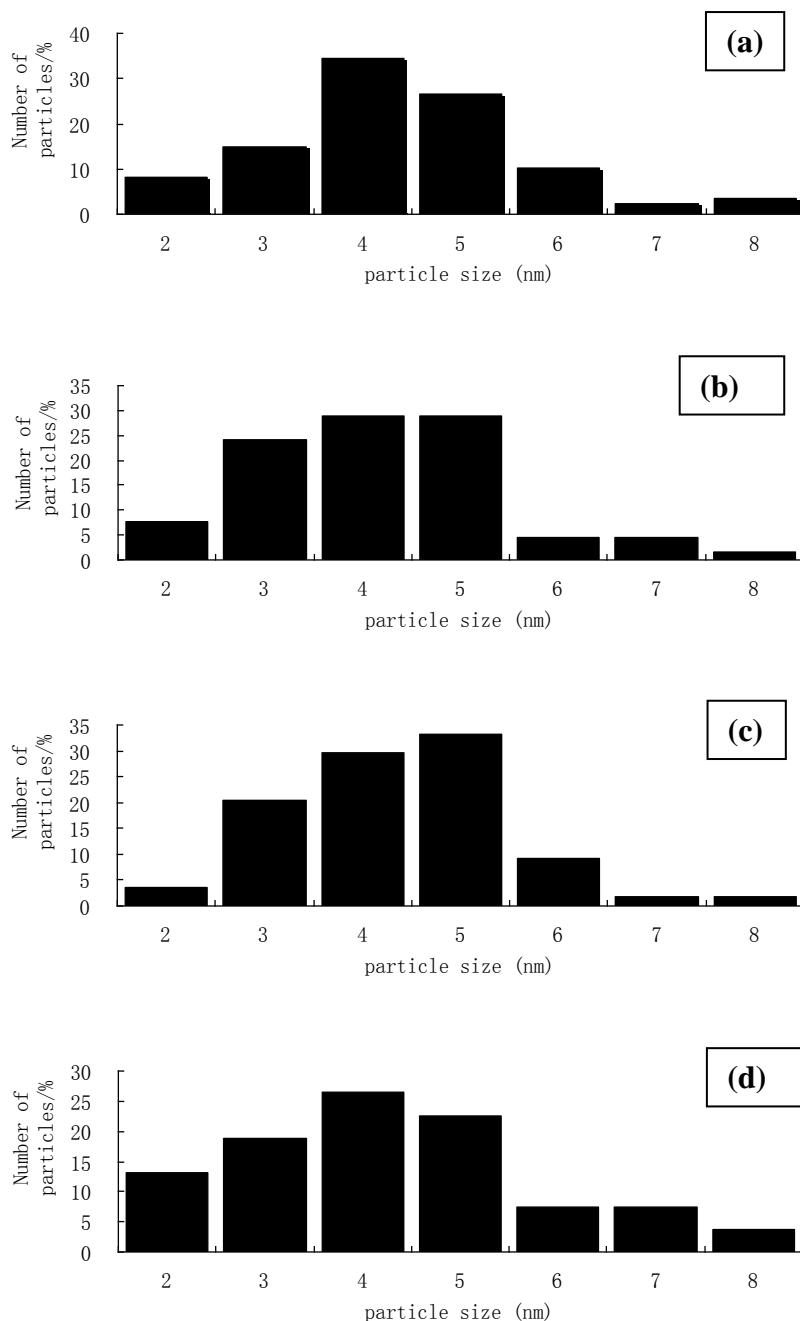
where *k* = 0.124 Å is a constant [14], and *a*<sub>PdRu</sub> and *a*<sub>Pd</sub> are the lattice parameters of pure Pd and PdRu, respectively. The value of *x*<sub>PdRu</sub> for Pd<sub>4</sub>Ru/C, Pd<sub>2</sub>Ru/C, PdRu/C, and PdRu<sub>2</sub>/C were 1.3%,

1.5%, 2.2%, and 2.5%, respectively. These low extent of alloying partially results from the low-temperature synthesis and the large lattice mismatch (9.19% between fcc Pd and hcp Ru), and thus presenting as an ideal model structure to study exclusively the effect of Ru composition in mixed-phase PdRu catalysts.



**Figure 2.** TEM images of (a) PdRu<sub>2</sub>/C, (b) PdRu/C, (c) Pd<sub>2</sub>Ru/C, and (d) Pd<sub>4</sub>Ru/C. The scale bar for all the figures corresponds to 20 nm.

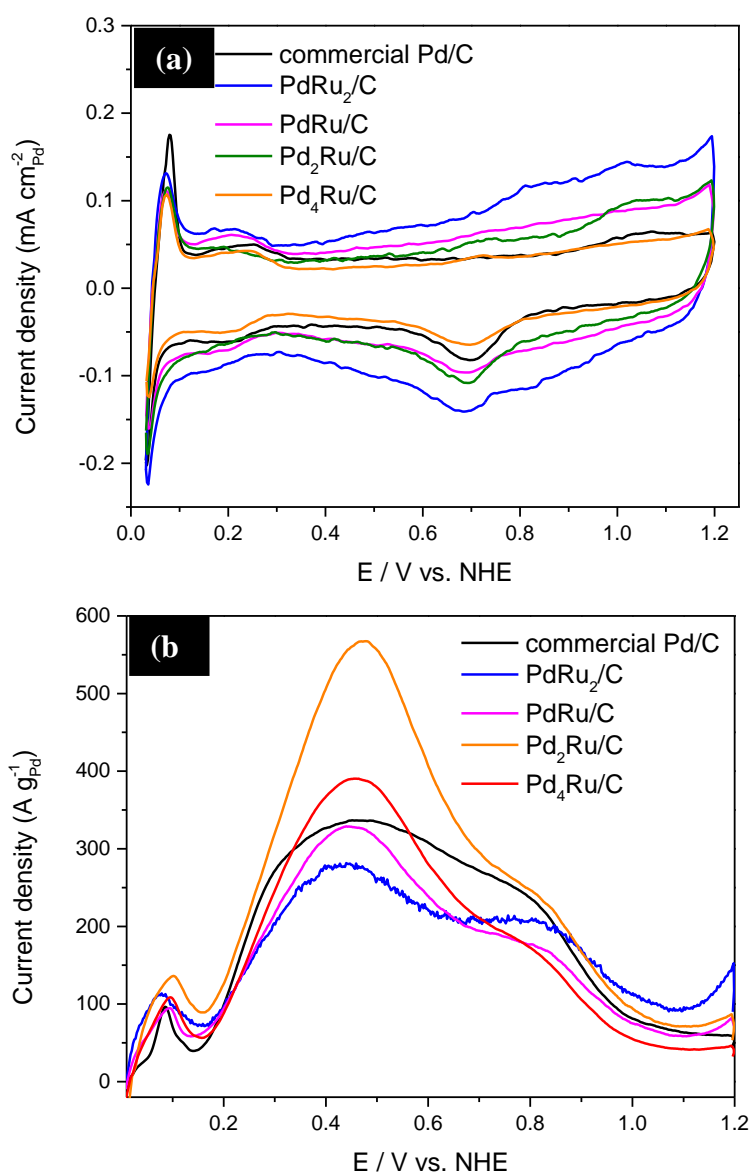
Fig. 2 displays the TEM images of the four Pd<sub>x</sub>Ru<sub>y</sub>/C catalysts. The images exhibited the agglomerated carbon support with primary particle size around 50 nm and well-dispersed Pd<sub>x</sub>Ru<sub>y</sub> nanoparticles. Sufficient number (ranging from several tens to even hundreds) of Pd<sub>x</sub>Ru<sub>y</sub> particles were analyzed and their particle size distributions were shown in Fig. 3. The average particle size is similar for all the samples: 4.36 nm for PdRu<sub>2</sub>/C, 4.18 nm for PdRu/C, 4.37 nm for Pd<sub>2</sub>Ru/C, and 4.30 nm for Pd<sub>4</sub>Ru/C. This result is consistent with the fact that these samples displayed similar ECSA values. It has been reported [14] that particle size of Pd<sub>x</sub>Ru<sub>y</sub> alloy, synthesized by a microwave assisted polyol process, decreased with increasing Ru ratio due to contraction of the fcc crystalline lattice. Our results, however, did not show a clear relation between Ru content and particle size of the Pd<sub>x</sub>Ru<sub>y</sub> particles synthesized by a co-precipitation method (because of their negligible extent of alloying). On the other hand, only at the lowest Ru content, i.e., in the Pd<sub>4</sub>Ru/C, large particles emerge as shown both in size distribution (Fig. 3d) and TEM image (Fig. 2d).



**Figure 3.** Particle size distribution of (a) PdRu<sub>2</sub>/C, (b) PdRu/C, (c) Pd<sub>2</sub>Ru/C, and (d) and (d) Pd<sub>4</sub>Ru/C.

Electrochemical characteristics of the Pd<sub>x</sub>Ru<sub>y</sub>/C and the commercial Pd/C were evaluated and results are shown in Fig. 4. The current densities for different samples in Fig. 4a have been normalized to the measured ECSA. All the curves showed distinct electrochemical peaks corresponding to hydrogen adsorption/desorption and oxides formation/reduction. However, CVs of Pd<sub>x</sub>Ru<sub>y</sub>/C catalysts exhibited less-resolved and broad peaks compared to the commercial Pd/C due to the non-alloying Ru in the catalysts [22]. The other salient feature of the Pd<sub>x</sub>Ru<sub>y</sub>/C catalysts is the oxides formation/reduction section (> 0.5 V) in the voltammograms, which expands almost proportionally with the Ru content. Besides, the onset oxidation potential of the PdRu<sub>2</sub>/C appears at only ~ 0.4 V,

which is 500 mV more negative than those of Pd/C and Pd<sub>4</sub>Ru/C samples. These results suggest that the Ru component in the particles, mostly in a single phase, helps generate surface oxides which may contribute to FAO, but also on the other hand block the surface preventing further electrochemical reactions. Fig. 4b showed the linear sweep voltammograms of the commercial Pd/C and the Pd<sub>x</sub>Ru<sub>y</sub>/C catalysts for FAO reaction. From the curves, all the Pd<sub>x</sub>Ru<sub>y</sub>/C catalysts showed the highest peak currents at around 0.48 V (vs. NHE) which is attributed to the direct pathway of FAO (i.e., formic acid directly to CO<sub>2</sub>). Among these catalysts, the Pd<sub>2</sub>Ru/C demonstrated a superior mass-specific current density (567 A g<sup>-1</sup>) that is 1.7 times higher than that of the commercial Pd/C (336 A g<sup>-1</sup>). Because Ru does not contribute to FAO reaction according to the previous report [22], we therefore attribute the enhancement exclusively to the structural change (i.e., the number of boundary sites between individual Pd and Ru phases), surface electronic coupling between Pd and Ru [5], as well as spillover of oxygen-containing species from Ru to Pd.



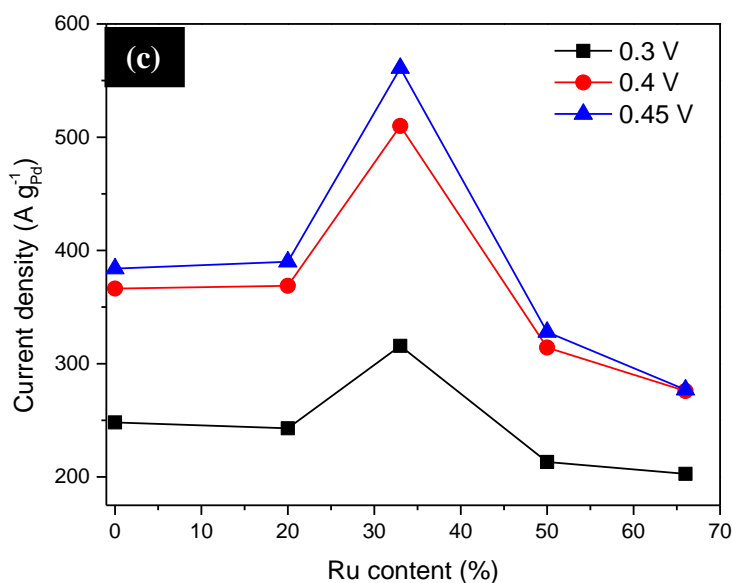


**Figure 4.** (a) The CV curves in 0.1M HClO<sub>4</sub> solution, (b) FAO CVs of Pd/C, PdRu<sub>2</sub>/C, PdRu/C, Pd<sub>2</sub>Ru/C, and Pd<sub>4</sub>Ru/C in 0.1M (HClO<sub>4</sub> and HCOOH) solution (only the anodic scans are shown), and (c) dependence of FAO activity of the Pd<sub>x</sub>Ru<sub>y</sub>/C on Ru content. The scan rate was 20 mV s<sup>-1</sup> in the CV curves. All the solutions were purged with Ar for 1 hr before the measurement.

Fig. 4b also shows a second anodic peak at around 0.85 V which is ascribed to FAO through an indirect pathway (i.e., CO as a reaction intermediate). The ratio of peak current densities (the one at 0.48 V to that at 0.85 V) seems to increase monotonically with the Ru content in the Pd<sub>x</sub>Ru<sub>y</sub>/C. This result suggests a transition in FAO reaction pathway from indirect to direct routes with increasing Ru content, possibly due to modulation of CO adsorption and oxidation by Ru [22].

In order to understand the implication of Ru content to the catalytic activity toward FAO, current densities in Fig. 4b were replotted in Fig. 4c against Ru content at 0.3 V, 0.4 V, and 0.45 V. The obtained volcano-shaped curves pointed out that the highest mass activity of the Pd<sub>x</sub>Ru<sub>y</sub>/C was achieved at 33 at% of Ru (i.e., Pd<sub>2</sub>Ru/C), which results from an optimum balance between fast CO removal by Ru and its blocking effect because Ru does not react with formic acid. To shed lights on the FAO mechanism, CO-stripping CV was employed to probe surface of the commercial Pd/C, Ru/C, and Pd<sub>x</sub>Ru<sub>y</sub>/C catalysts. The black curves in Fig. 5 show the initial anodic scan after CO was adsorbed on the catalysts, and the red curves correspond to the anodic scans afterward. For all the Pd-Ru catalysts, the broad peaks near ~ 1.05 V may be caused by oxidation of citric acid [23] that was used during catalyst synthesis, and some residue possibly remained on the catalyst surface. In addition, there is no noteworthy anodic peak for Ru/C, which confirms its inertness toward CO oxidation [14]. The PdRu<sub>2</sub>/C displays a much lower CO oxidation peak potential at 0.65 V than 0.92 V of the commercial Pd/C, suggesting a much weaker CO adsorption strength. Other Pd<sub>x</sub>Ru<sub>y</sub>/C catalysts, such as the Pd<sub>4</sub>Ru/C (0.82 V), Pd<sub>2</sub>Ru/C (0.81 V), and PdRu/C (0.832 V), also exhibited lower CO oxidation peak potentials than the Pd/C, confirming that the enhancement in CO oxidation of the catalysts is attributed to Ru [13].

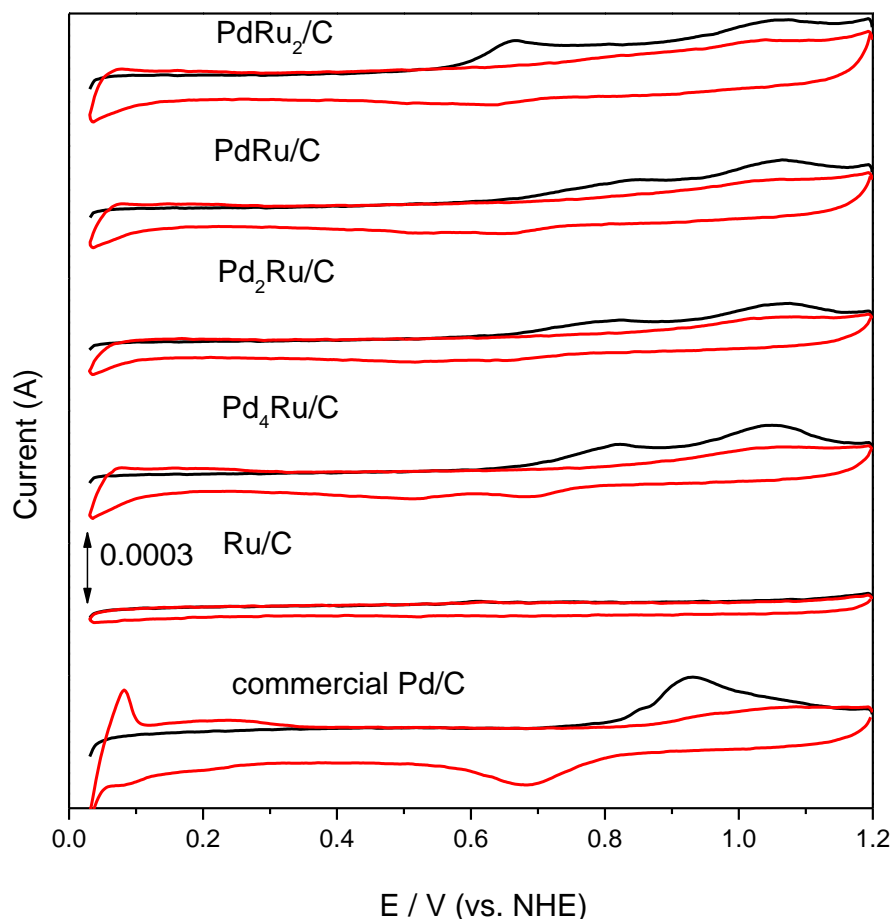


**Figure 5.** CO-stripping CVs of the commercial Pd/C, Ru/C, and the synthesized Pd<sub>x</sub>Ru<sub>y</sub>/C. The black curves show the first scan and red curves correspond the second scan. The scan rate is 20 mV s<sup>-1</sup>.

According to our previous report [5], the trace amount CO may be generated in FAO via the dehydration pathway ( $\text{HCOOH} \rightarrow \text{CO}_{\text{ads}} + \text{H}_2\text{O} \rightarrow \text{CO}_2 + 2\text{H}^+ + 2\text{e}^-$ ) and absorb on the active sites of Pd catalysts, which could be facily removed with the help of Ru. This suggests the important role of Ru in FAO: 1) Ru helps oxidize and remove CO from Pd surface through spillover of oxygen-containing species, and 2) most important, Ru also assists diverting FAO reaction pathway more toward a direct route.

Durability of the Pd based catalysts was studied by potential cycling between -0.02 V and 1.2 V in mixed solutions containing 0.1 M formic acid and 0.1 M HClO<sub>4</sub>. In Fig. 6 both the FAO current density at the first anodic peak and that at 0.3 V were normalized to their initial values so that the relative decay rate can be studied. Fig. 6a shows that the commercial Pd/C maintained the higher value after 100 cycles with only ~15% loss of peak current density than those of Pd<sub>2</sub>Ru/C (~40% loss), Pd<sub>4</sub>Ru/C (~40% loss), PdRu/C (~50% loss), and PdRu<sub>2</sub>/C (~57% loss), suggesting adding Ru to Pd may not efficiently improve durability after long cycles.

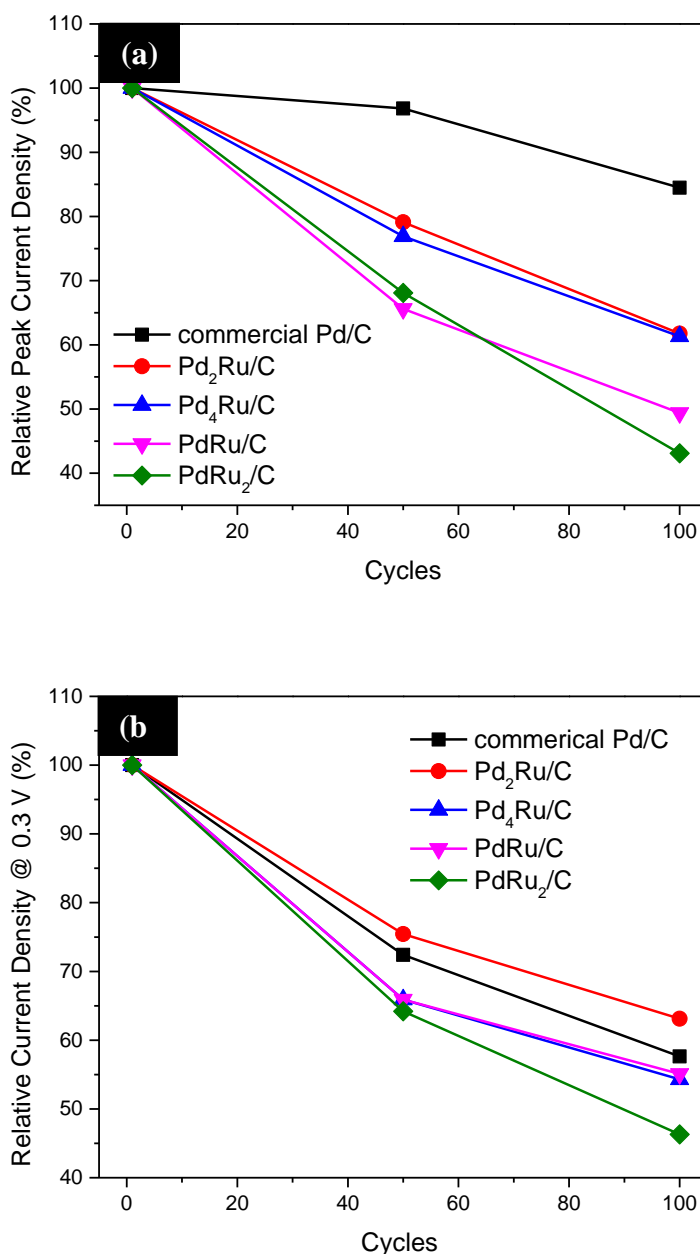


**Figure 6.** Normalized current density (a) at the anodic FAO peak potential and (b) at 0.3 V for the commercial Pd/C and Pd<sub>x</sub>Ru<sub>y</sub>/C catalysts during potential cycles. The scan rate for the whole test was at 50 mV s<sup>-1</sup>.

Nevertheless, even after 100 cycles the Pd<sub>2</sub>Ru/C still shows 30% higher mass-specific activity (at 364.50 A g<sup>-1</sup>) than the commercial Pd/C (at 275.13 A g<sup>-1</sup>). As previously reported [10, 24], Ru could be corroded and forms RuO<sub>2</sub> or RuO<sub>x</sub>H<sub>y</sub> at higher potentials (> 0.45 V), resulting in decrease of catalytic ability of Pd-Ru catalysts. To our surprise, the relative current density at 0.3 V for Pd<sub>2</sub>Ru/C was found to be slightly lower than that of the commercial Pd/C after 100 cycles as shown in Fig. 6b. The former still preserves ~63% (at 259.62 A g<sup>-1</sup>) of its initial current density at 0.3 V, while the latter retains ~58% (at 157.21 A g<sup>-1</sup>) of its initial value.

#### 4. CONCLUSIONS

The Pd<sub>x</sub>Ru<sub>y</sub>/C nanoparticles were successfully synthesized via simultaneous reduction of PdCl<sub>2</sub> and RuCl<sub>3</sub> on carbon support using NaBH<sub>4</sub>. The XRD results showed the peak shift of Pd (220), indicating the contraction of Pd fcc structure by adding Ru. The TEM images displayed well-distributed spherical-shaped Pd<sub>x</sub>Ru<sub>y</sub> nanoparticles on the carbon support. Electrochemical evaluation indicated that the Pd<sub>x</sub>Ru<sub>y</sub>/C nanoparticles (x:y =4:1 and 2:1) exhibited excellent catalytic activities in formic acid oxidation, stronger CO oxidation ability, and long-term durability than the commercial Pd/C. Notably, the Pd<sub>2</sub>Ru/C catalyst in this study displayed the best catalytic properties due to the interaction between Pd and Ru, which enhances the CO oxidation and further improves the FAO ability. This suggests the important role of Ru in FAO: 1) Ru helps oxidize and remove CO from Pd surface, and 2) most important, Ru also assists diverting FAO reaction pathway more toward a direct route.

#### ACKNOWLEDGEMENTS

Financial support to Electrochemical Energy Center at UTA is greatly acknowledged. WM would like to acknowledge Jiangsu Normal University and the National Natural Science Foundation of China (No. 21376113 ) for financial support of this work. CH and ZW would like to thank Dr. J-C Jiang and D. Yan for the technical support from UTA Characterization Center for Materials and Biology (CCMB).

#### References

1. C. Rice, S. Ha, R. Masel, P. Waszczuk, A. Wieckowski and T. Barnard, *J. Power Sources*, 111 (2002) 83
2. P. Waszczuk, A. Wieckowski, P. Zelenay, S. Gottesfeld, C. Coutanceau, J.-M. Léger and C. Lamy, *J. Electroanal. Chem.*, 511 (2001) 55
3. Z. Liu, L. Hong, M. P. Tham, T. H. Lim and H. Jiang, *J. Power Sources*, 161 (2006) 831
4. Y. Lu and W. Chen, *J. Phys. Chem. A*, 114 (2010) 21190
5. C. Hsu, C. Huang, Y. Hao and F. Liu, *Electrochem. Commun.*, 23 (2012) 133
6. X. Wang and Y. Xia, *Electrochem. Commun.*, 10 (2008) 1644
7. C. Du, M. Chen, W. Wang, G. Yin and P. Shi, *Electrochem. Commun.*, 12 (2010) 843
8. C. Xu, Y. Liu, J. Wang, H. Geng and H. Qiu, *J. Power Sources*, 199 (2012) 124
9. C. Hsu, C. Huang, Y. Hao and F. Liu, *J. Power Sources*, 243 (2013) 343
10. Z. Zhang, J. Liu, J. Gu, L. Su and L. Cheng, *Energ. Environ. Sci.*, 7 (2014) 2535
11. S. Shen, T. Zhao and J. Xu, *Electrochim. Acta*, 55 (2010) 9179
12. Y. Chen, L. Zhuang and J. Lu, *Chin. J. Catal.*, 28 (2007) 870
13. J. Guo, T. Zhao, J. Prabhuram, R. Chen and C. Wong, *Electrochim. Acta*, 51 (2005) 754
14. Z. Liu, X. Zhang and S. W. Tay, *J. Solid State Electrochem.*, 16 (2012) 545
15. Q. Lu, B. Yang, L. Zhuang and J. Lu, *J. Phys. Chem. B*, 109 (2005) 1715
16. A. Neto, R. Verjullo-Silva, M. Linardi and E. Spinacé, *Int. J. Electrochem. Sci.*, 4 (2009) 954
17. M. R. Tarasevich, Z. R. Karichev, V. A. Bogdanovskaya, E. N. Lubnin and A. V. Kapustin, *Electrochem. Commun.*, 7 (2005) 141
18. D. Wu, Z. Zheng, S. Gao, M. Cao and R. Cao, *Phys. Chem. Chem. Phys.*, 14 (2012) 8051
19. W. Xu, T. Lu, C. Liu and W. Xing, *J. Phys. Chem. B*, 109 (2005) 14325
20. J. I. Hur, D. D. Meng and C.-J. Kim, *Journal of Microelectromechanical Systems*,

21 (2012) 476

21. L. Sun, D. Cao and G. Wang, *J. Appl. Electrochem.*, 38 (2008) 1415
22. L. Ma, H. He, A. Hsu and R. Chen, *J. Power Sources*, 241 (2013) 696
23. K. Honeychurch, L. Gilbert and J. Hart, *Anal. Bioanal. Chem.*, 396 (2010) 3103
24. B. r. Wickman, Y. E. Seidel, Z. Jusys, B. Kasemo and R. J. r. Behm, *ACS Nano*, 5 (2011) 2547

© 2016 The Authors. Published by ESG ([www.electrochemsci.org](http://www.electrochemsci.org)). This article is an open access article distributed under the terms and conditions of the Creative Commons Attribution license (<http://creativecommons.org/licenses/by/4.0/>).